Geotextiles and Geomembranes 28 (2010) 374–385

Contents lists available at ScienceDirect

Geotextiles and Geomembranes

journal homepage: www.elsevier.com/locate/geotexmem

Static liquefaction of fibre reinforced sand under monotonic loading

E. Ibraim [a,*], A. Diambra [a], D. Muir Wood [a], A.R. Russell [b]

[a] Department of Civil Engineering, University of Bristol, Queen's Building, University Walk, Bristol BS8 1TR, United Kingdom
[b] School of Civil and Environmental Engineering, University of New South Wales, Sydney, NSW 2052, Australia

ARTICLE INFO

Article history:
Received 24 May 2009
Received in revised form
24 September 2009
Accepted 2 December 2009
Available online 16 February 2010

Keywords:
Sand
Fibre reinforced sand
Triaxial test
Compression
Extension
Static liquefaction

ABSTRACT

This paper explores the possibility of improving the monotonic undrained response of a loose clean sand which normally appears susceptible to the phenomenon of static liquefaction by mixing the sand with discrete flexible fibres. It is shown that the reinforcement inclusions reduce the potential for the occurrence of liquefaction in both compression and extension triaxial loadings and convert a strain softening response (typical for a loose unreinforced sand) into a strain hardening response. Fibre orientation distribution and the apparent sand matrix densification due to the presence of fibres in the voids appear important for the fibre reinforced soil behaviour. Normalisation of the effective stress paths with the mean effective stress at the end of consolidation shows a common path once the characteristic state is reached irrespective of the fibre concentration. The mobilised angles of friction coming from the slopes of the stress paths at large strains are very different for compression and extension and this is a consequence of the anisotropic nature of the distribution of fibre orientations. When full liquefaction of reinforced specimens is induced by strain reversal, the lateral spreading of soil seems to be prevented. Analytical developments including the key aspect of fibre orientation distribution, have shown that once the tensile contribution of fibres has been taken out of the composite stresses, the experimental data in the stress plane for all the tests at large shear strains nicely collapse onto a unique line corresponding very closely to the mobilised steady state or critical state angle of friction of the tested sand.

1. Introduction

Since the pioneering work of Bjerrum et al. (1961) and Castro (1969), liquefaction of granular soils has been intensively studied especially in the laboratory (Castro and Christian, 1976; Vaid and Chern, 1983; Konrad, 1990; Chu, 1991; Lade, 1992; Hyodo et al., 1994; Doanh et al., 1997; Doanh and Ibraim, 2000, among others). Liquefaction under monotonic undrained loading, commonly called 'static liquefaction', is typically associated with loose and very loose saturated sands and sand–silt mixtures while in situ and under relatively low stress conditions, and may be defined as a large reduction of mean effective pressure induced by a persistent generation of pore pressures. Large strains develop with a significant drop of the undrained shear strength which eventually stabilises around a steady state condition (Poulos, 1981). Several failures of natural loose saturated sandy slopes, earth dams or hydraulically filled submarine berms have been attributed to the 'static liquefaction' of the soil (Castro and Poulos, 1977; Lindenberg and Koning, 1981; Sladen et al., 1985; Kramer and Seed, 1988). In some cases, a trigger mechanism such as a minor disturbance in the form of vibrations due to man-made activities or earthquakes of small intensities, local erosion, tidal variations or overloading imposed by additional fill, has been proposed as the origin of the sudden increase of pore-water pressures (Lade, 1993).

The present paper explores through a series of laboratory experiments the prospect of altering the undrained monotonic response of a loose clean sand to reduce its liquefaction potential by mixing the sand with short flexible fibres. Reinforcing sand with flexible discrete fibres does not represent a new technique in geotechnical engineering. However, no study has been reported concerning the undrained monotonic behaviour of fibre reinforced sands or on the effect of fibre inclusions on the static liquefaction response of sand.

2. Fibre reinforced sand: research background

It is well known that the roots of surface vegetation contribute to the stability of slopes by adding strength to the near-surface soils in which the effective stress is low (Wu et al., 1988; Ekanayake and Phillips, 2002; Greenwood et al., 2004; Greenwood, 2006; Danjon et al., 2007). Laboratory and some in situ pilot test results (Jewell and Wroth, 1987; Palmeira and Milligan, 1989; Al Refeai, 1991;

* Corresponding author. Tel.: +44 117 928 8328; fax: +44 117 928 7783.
E-mail address: erdin.ibraim@bristol.ac.uk (E. Ibraim).

0266-1144/$ – see front matter © 2009 Elsevier Ltd. All rights reserved.
doi:10.1016/j.geotexmem.2009.12.001

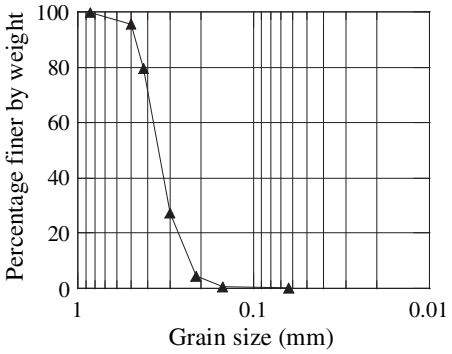

Fig. 1. Grain size distribution of Hostun RF sand.

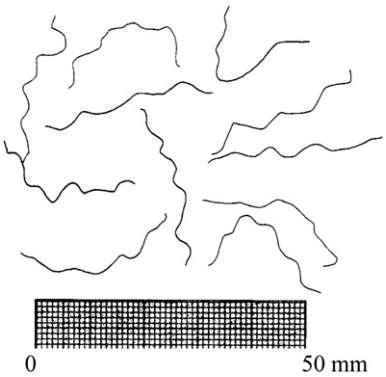

Fig. 2. Individual Loksand™ flexible polypropylene crimped fibres.

Michałowski and Zhao, 1996; Consoli et al., 1998, 2007, 2009; Santoni and Webster, 2001; Tingle et al., 2002; Zornberg, 2002; Park and Ann Tan, 2005; Singh Chauhan et al., 2008, among others) have led to encouraging conclusions concerning the potential use of flexible fibres for the reinforcement of fine granular materials – providing an artificial replication of the effects of vegetation.

Monotonic loading in shear box tests, consolidated and unconfined drained triaxial compression tests have shown that shear strength is increased and post-peak strength loss is reduced when discrete fibres are mixed with the soil (Gray and Ohashi, 1983; Maher and Ho, 1994; Yetimoglu and Salbas, 2003; Ibraim and Fourmont, 2007, among others). The presence of fibres appears to prevent the formation of shear bands and loss of fabric in the directions of tensile strain (Ibraim et al., 2006; Sivakumar Babu et al., 2008). The effectiveness of the reinforcement is influenced by fibre properties: type, volume fraction, length, aspect ratio, modulus of elasticity, together with orientation and also soil characteristics including particle size, shape, and gradation, as well as stress level and soil (matrix) density. At high confining stresses, the compressive strength of the reinforced sand appears to increase linearly with the concentration of fibres (the fibre concentration is conveniently expressed in terms of weight fraction of dry sand); for low values of the confining stress, this increase approaches an asymptotic upper limit (Gray and Al-Refeai, 1986; Al Refeai, 1991; Ranjan et al., 1996; Murray et al., 2000). Also, for a given fibre concentration, strength, as expressed by the major principal stress at failure, increases linearly with fibre aspect ratio (fibre length over fibre diameter). It has also been noted that for a given confining stress, the strength of the reinforced sand increases with reducing average grain size D_{50} (Gray and Al-Refeai, 1986; Maher and Gray, 1990). Also, an increase in coefficient of uniformity ($C_u = D_{60}/D_{10}$) results in higher contribution of fibres to strength.

The important influence of fibre orientation on the mechanical response of fibre reinforced soils has been experimentally investigated in tests with controlled orientations of fibres (Jewell and Wroth, 1987; Palmeira and Milligan, 1989; Michałowski and Čermák, 2002). Many experimental studies implicitly assume that the fibres are randomly oriented throughout the soil mass and, as reported by others (Michałowski, 2008, for example), there has been very little effort to check this hypothesis experimentally. However, in recent experimental and analytical work, Diambra et al. (2007a) found that the most common procedure for preparing reinforced specimens, moist tamping, leads in fact to preferred subhorizontal orientation of fibres. The same conclusion is found for specimens prepared with vibration (Diambra et al., 2008a). Since rotations of principal stress and strain axes almost always occur within a soil mass (Arthur et al., 1980, for example), the consequence of an assumed isotropy of fibre orientation would be the overestimation of soil design strength for certain loadings and underestimation for others.

Most of the studies mentioned above have focused on the analysis of strength and deformation characteristics of saturated fibre reinforced sands under drained loading conditions. For granular materials, whether reinforced or not, the stability under most normal working conditions is controlled by drained strength parameters. However, a rapid loading due to an earthquake or a static collapse may create undrained loading conditions and large pore pressures may be induced in the soil mass, especially if the soil response has a strain-softening tendency.

Studies on liquefaction resistance of reinforced soils have been so far limited to the cyclic liquefaction of sand, fly ash or clay reinforced with geotextiles and short fibres (Vercueil et al., 1997; Li and Ding, 2002; Unnikrishnan et al., 2002; Boominathan and Hari, 2002). Fibre inclusions increase the number of cycles required to cause liquefaction during undrained loading (Noorany and Uzdavines, 1989; Maher and Woods, 1990; Krishnaswamy and Isaac, 1994). However, the data generated in these studies are only suitable for empirical interpretation. Undrained shear strength characteristics of a mixture of clay and rubber fibres (tire buffings) have recently been presented by Özkul and Baykal (2007).

In this paper triaxial test results are presented for a very fine sand reinforced with discrete crimped polypropylene fibres. No preferential orientation of fibres is given other than that generated by the normal fabrication process. Only loose specimens susceptible to static liquefaction are considered and although triaxial test results in drained conditions are discussed, the analysis is focused on the undrained behaviour in both triaxial compression and triaxial extension. Additional test results and characterisation of this composite material are presented by Ibraim and Fourmont (2007), Diambra et al. (2007b, in press).

3. Experimental programme and procedures

3.1. Materials

Hostun RF (S28) sand with a mean grain size, $D_{50} = 0.38$ mm, coefficient of uniformity, $C_u = D_{60}/D_{10} = 1.9$, coefficient of gradation, $C_g = (D_{30})^2/(D_{10}D_{60}) = 0.97$, maximum and minimum void ratio, $e_{max} = 1.041$, $e_{min} = 0.648$ and specific gravity $G_s = 2.65$ has been used in this study. Fig. 1 shows the grain size distribution of Hostun RF sand. Loksand™ flexible polypropylene crimped fibres have been used (Fig. 2). These fibres act predominately in tension and their properties as provided by the manufacturer together with the averaged tensile strength obtained through a series of 15 tension tests are listed in Table 1.

Table 1
Characteristics of Loksand™ fibres.

Length (mm)	Diameter (mm)	Tensile strength (MPa)	Specific gravity, G_f	Elongation at break	Moisture regain
35	0.1	225	0.91	160%	<0.1%

In this paper, the concentration of fibres included in a composite is defined as a proportion of dry weight of sand $w_f = W_f/W_s$, where W_f is the weight of fibres and W_s is the weight of the dry sand.

3.2. Specimen preparation

Unreinforced and fibre reinforced specimens were prepared using a moist tamping technique. This fabrication method is commonly used in laboratory studies of fibre reinforced sands and it has the advantage of a good control of specimen density while preventing the segregation of fibres. It eventually produces a soil-fibre fabric which resembles that of compacted reinforced soils in the field. Preliminary compaction tests (Fig. 3) using a modified Proctor test have shown that for a given compaction effort the maximum dry density of reinforced sand decreases with increasing fibre content (w_f) whereas the optimum moisture content (around 10%) is independent of the amount of the fibres used (Ibraim and Fourmont, 2007). More compaction energy appears necessary to produce specimens with higher fibre contents at a given dry density. This must be considered along with improvements in performance and the use of low density reinforced soils in cost–benefit analyses.

Specimens for triaxial testing with diameter 70 mm and height 70 mm were prepared in three layers of equal height. The optimum moisture content of 10% was used for the fibre/sand mixing process; further details of the procedure are given by Ibraim and Fourmont (2007). In developing the fabrication procedure, prototype reinforced and unreinforced specimens made in a transparent Perspex tube did not show any significant over-compaction effects during the formation of the higher layers.

For all the specimens presented in this study, the quantity of sand, W_s, was kept unchanged when different proportions of fibres were added. The target fabrication void ratio chosen for unreinforced specimens was around 1.0. It should be noted that there is a limit to the proportion of fibres that can be added to the sand (dry sand weight, W_s, and specimen volume both kept constant) if the moist tamped composite is to be effectively prepared. The maximum fibre content, w_f, that can be employed for this target fabrication void ratio is approximately 1% (Ibraim and Fourmont, 2007). For the specimens tested in compression, three different concentrations of fibres – 0.3%, 0.6% and 0.9% – were used whereas only two, 0.3% and 0.6%, were used for those specimens tested in extension.

3.3. Triaxial test conditions

Conventional drained and undrained triaxial compression and extension tests were conducted on unreinforced and reinforced isotropically consolidated specimens. Three different consolidation pressures – 30, 100 and 200 kPa – were used. A complete list of tests including the void ratios at the end of isotropic consolidation, fibre contents (w_f), consolidation pressures and test type is given in Table 2. Table 2 presents alternative calculations of the void ratios when (i) the volume occupied by fibres is 'attached' to the volume of voids, e_m, and when (ii) the volume occupied by fibres is 'attached' to the sand matrix volume, e_{fm}. As can be observed, the differences between these two values of the void ratio are very small, typically less than 0.05. It is also known that some densification inherently occurs during the saturation process of low density specimens; however, no correction was applied to the initial specimen volume though the presence of fibres may limit the collapse of the sand structure.

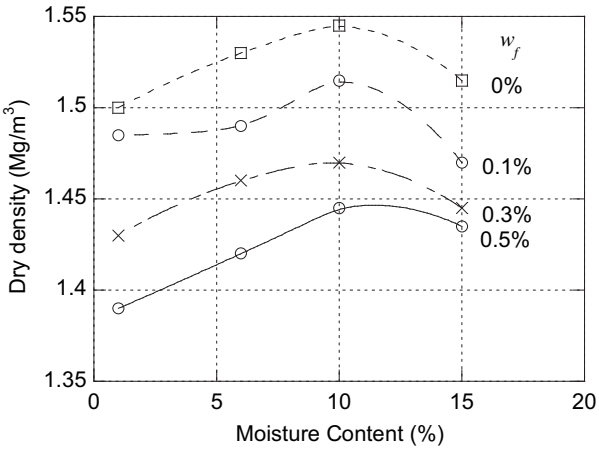

Fig. 3. Compaction test results on polypropylene fibre reinforced and unreinforced Hostun RF sand (w_f represents the fibre content).

The specimens were saturated using the CO_2 method together with water back pressure up to 300 kPa. Values of B (Skempton coefficient) of at least 0.97 were deemed to give indication of sufficient water saturation for undrained tests (Lindenberg and Koning, 1981). Conventional axial and volumetric strain measurement systems were used together with an internal load cell. Further details are given by Diambra et al. (2007b).

Enlarged and lubricated specimen ends of 100 mm diameter consisting of silicone grease and latex rubber discs were used at the bottom (two discs) and at the top (three discs). A homogeneous specimen shape seemed to be well preserved up to or well beyond 20% axial strain (ε_a) in compression; in extension necking of the sample was only visible after 10–12% axial straining. It is well known that the use of lubricated ends amplifies the bedding errors for the axial strain response, but no local axial measurement system was used nor were corrections applied to the results since the small strain response of fibre reinforced soil was beyond the scope of this experimental study. The calculation of membrane penetration effects showed these to be negligible, as also observed in previous studies by Ibraim (1998) for similar sand, specimen dimensions and membrane thickness. However, the effect of the stiffness of the membrane has been taken into account and the results corrected following the recommendations of ASTM (1988) Soils and Rocks D-18 Committee.

The contact between the top cap of the specimen and the loading ram is similar to that used by Mohkam (1983) and Ibraim (1998) (Fig. 4a). The contact is made after a sample has consolidated and requires a two stage process as schematically shown in Fig. 4b and c. As a result of the initial adjustments of the contact between the loading ram and the top cap of the specimen, the initial part of the axial loading for some undrained triaxial tests showed a sudden pore pressure increase with clear effects on the estimation of the initial effective stresses. However, as the sample was further sheared in compression or extension, this effect was found to be transitory and disappeared very quickly. No quantitative interpretation of the initial undrained response is included in this paper.

Table 2
List of the triaxial tests performed.

Test	e_m	e_{fm}	w_f (%)	p_c^* (kPa)	Compression(C) Extension (E) Drained(D) Undrained (U)	$(q^*/p^*)^a$	$\phi_m^{*}(^\circ)^b$
CD100-00	0.991	0.991	0	100	C, D	1.36	33.7
CD100-03	0.983	0.966	0.3			1.73	42.2
CD100-06	0.979	0.945	0.6			1.98	48.1
CD100-09	0.987	0.936	0.9			2.26	55.2
ED100-00	0.989	0.989	0	100	E, D	−1.01	37.4
ED100-03	0.988	0.971	0.3			−1.08	41.2
ED100-06	0.985	0.951	0.6			−1.13	44.1
CU030-00	1.015	1.015	0	30	C, U	1.35	33.4
CU030-03	1.007	0.990	0.3			2.02	49.1
CU030-06	1.011	0.976	0.6			2.30	56.2
CU030-09	1.018	0.966	0.9			2.44	60.1
CU100-00	0.999	0.999	0	100	C, U	1.46	36.0
CU100-03	0.981	0.964	0.3			1.82	44.3
CU100-06	0.993	0.959	0.6			2.11	51.3
CU100-09	0.991	0.940	0.9			2.30	56.2
CU200-00	0.985	0.985	0	200	C, U	1.34	33.2
CU200-03	0.980	0.963	0.3			1.82	44.3
CU200-06	0.967	0.933	0.6			1.96	47.6
CU200-09	0.973	0.923	0.9			2.16	52.6
EU030-00	0.995	0.995	0	30	E, U	−1.00	36.9
EU030-03	0.985	0.968	0.3			−1.11	42.9
EU030-06	0.991	0.957	0.6			−1.03	38.4
EU100-00	0.964	0.964	0	100	E, U	−0.92	32.9
EU100-03	0.953	0.936	0.3			−1.02	37.9
EU100-06	0.962	0.928	0.6			−1.02	37.9
EU200-00	0.967	0.967	0	200	E, U	−0.99	36.4
EU200-03	0.951	0.934	0.3			−1.00	36.9
EU200-06	0.962	0.928	0.6			−1.08	41.2

[a] q^*/p^* = stress ratio at $\varepsilon_q = 20\%$ in compression and $\varepsilon_q = 10\%$ in extension.
[b] $\phi_m^*(^\circ)$ = mobilised angle of friction at $\varepsilon_q = 20\%$ in compression and $\varepsilon_q = 10\%$ in extension.

4. Experimental results

4.1. Notation

In presenting and discussing the experimental results the notation of Diambra et al. (in press) for axisymmetric triaxial conditions has been adopted. Thus, p and q are respectively the total mean and deviatoric stresses acting on the composite with $p = p^* + u$ and p^* the effective mean stress, where u is the pore water pressure. Although the deviator stress is unaffected by pore water pressure, for uniformity of notation, the deviator stress on the composite will be denoted as q^*. The strain variables of the composite are the volumetric strain, ε_v, and shear strain, ε_q. These stress and strain quantities are related to axial and radial stresses and strains according to:

$$p = \frac{\sigma_a + 2\sigma_r}{3}, \quad q = \sigma_a - \sigma_r, \quad \varepsilon_v = \varepsilon_a + 2\varepsilon_r, \quad \varepsilon_q = \frac{2}{3}(\varepsilon_a - \varepsilon_r) \qquad (1)$$

where subscripts a and r denote the axial and radial components respectively.

If $q^*/p^* = M$, the Mohr-Coulomb mobilised angle of friction ϕ_m^* is defined by:

$$\sin\phi_m^* = \frac{3M_c}{6 + M_c}, \quad \sin\phi_m^* = \frac{-3M_e}{6 + M_e} \qquad (2)$$

where the subscripts c and e indicate triaxial compression and triaxial extension respectively.

The effective stress state of the composite, $\boldsymbol{\sigma}^* = [p^*, q^*]^T$, is the main focus of this study. However, for the development of constitutive models for the fibre reinforced soil (see Diambra et al., in press) it is necessary to use a mixture rule to divide the stresses into components representing the effective stress states of the sand matrix $\boldsymbol{\sigma}' = [p', q']^T$ and fibres $\boldsymbol{\sigma}_f = [p_f, q_f]^T$:

$$\boldsymbol{\sigma}^* = \nu_m \boldsymbol{\sigma}' + \nu_f \boldsymbol{\sigma}_f \qquad (3)$$

where the volumetric concentration factors ν_m and ν_f (for the soil matrix and the fibres, respectively) scale the individual components and are defined as:

$$\nu_m = \frac{V_s + V_v}{V} = \frac{V - V_f}{V}; \quad \nu_f = \frac{V_f}{V}; \text{ and } \nu_m + \nu_f = 1 \qquad (4)$$

and V, V_v, V_s and V_f are the volumes of the composite, voids, sand matrix and fibres, respectively (see Diambra et al., in press for a more detailed discussion). Note also that in definition of ν_m, the volume of voids (excluding the part occupied by the fibres) is considered to be part of the volume of sand matrix. For an unreinforced soil, $\nu_f = 0$, $\boldsymbol{\sigma}_f = 0$, $\nu_m = 1$ and $\boldsymbol{\sigma}^* = \boldsymbol{\sigma}' = [p', q']^T$ represents the effective stress in the conventional way.

4.2. Drained triaxial tests

Typical results of drained triaxial compression and extension tests on isotropically consolidated unreinforced and reinforced specimens at a consolidation pressure of 100 kPa are presented in Fig. 5 where the variations of the deviatoric stress, $q = q^*$, and the volumetric strain, ε_v, are presented with the shear strain, ε_q. Further drained triaxial test results are presented by Diambra et al. (in press).

In compression, the contribution of fibres to the strength of the composite is evident: except for the very small strain domain for

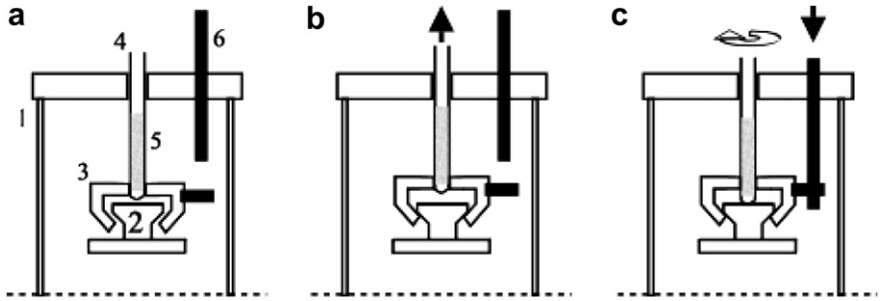

Fig. 4. (a) Different components used to connect the top cap to the loading ram: triaxial cell (1), specimen top cap (2), connection cap (3), axial loading ram (4), thread (5), rigid bar (6). (b) Connection stage 1 involves making contact between (2) and (3). (c) Connection stage 2 involves pushing down (6) then screwing down (4) until it makes contact with (2) while (3) is kept in a fixed position due to the contact with (6).

which, as noted, very precise measurements were not available, the deviatoric response was consistently higher when the concentration of fibres was higher. At 20% axial strain and with $w_f = 0.9\%$, the deviator stress was found to reach almost 300% increase compared with the unreinforced sand. The reinforced specimens show a somewhat bilinear stress–strain relationship and it appears that, even though some tests were taken to shear strains of 30–40%, the deviator stress is still increasing. Similar results have been presented by Ranjan et al. (1996), Sway and Bang (2007) for sand specimens reinforced with polypropylene fibres of high tensile strength. It appears that the fibres have a significant ability to withstand tension within the sand matrix without breakage or plastic deformations, as confirmed, in our case, by visual inspection of fibres exhumed from the specimens after each test.

In triaxial extension, the contribution of fibres to the deviatoric response appears to be very limited: the stress–strain relationships for reinforced specimens are almost identical to those for unreinforced specimens (Fig. 5a). In triaxial compression the deviatoric strength increase for 0.6% fibre content compared with the unreinforced sand reaches 180–200%, but only 8–10% increase in strength is recorded for the extension tests. The strength response of the composite in extension therefore appears to be largely controlled by the sand matrix. As shown by Diambra et al. (2007a), the method of fabrication leaves most fibres oriented in sub-horizontal directions, whereas the vertical direction is the direction of tensile strain in a triaxial extension test. These macro results clearly confirm these findings and emphasise the importance of considering the effect of fibre orientation on the performance of fibre reinforced sands. The strength increases provided by fibres are not isotropic. Rather, the effectiveness of fibres is higher when they are present in the direction of tensile strains.

The volumetric behaviour of unreinforced and reinforced specimens is presented in Fig. 5b. While the volumetric responses for unreinforced sand, in both compression and extension, show initial contraction and only limited eventual dilation at large strains (greater contraction in compression than in extension), which is a typical pattern of a low density sand, the volumetric behaviour of the reinforced sand approaches the characteristic response of a dense granular soil (even though the void ratio does not change significantly when fibres are added, see Table 2). After an initial reduction in volume, less significant than for the unreinforced sand, there is volumetric dilation with the dilatancy increasing with the fibre content. Similar results have been observed by Ibraim and Fourmont (2007) in direct shear tests performed on the composite material. For a given fibre content, the dilatancy is higher in extension than in compression. These results suggest that the volumetric response of the composite could be a consequence of an apparent densification mechanism of the sand matrix resulting from the presence of the fibres in the voids. In fact constitutive modelling developments (Diambra et al., 2008b; Diambra, in press) have found that the stress–strain behaviour is most accurately simulated when the global void ratio is divided into two parts: one belonging to the matrix and the other to the fibres. In other words, the fibres 'steal' voids from the matrix for themselves – hence the additional matrix densification.

The change of the volumetric response from contractive for the unreinforced sand to dilative for the reinforced one is an important characteristic which would be expected to influence potential for the occurrence of static liquefaction. It may significantly alter the stress changes required to build up sufficient pore water pressure for liquefaction to occur.

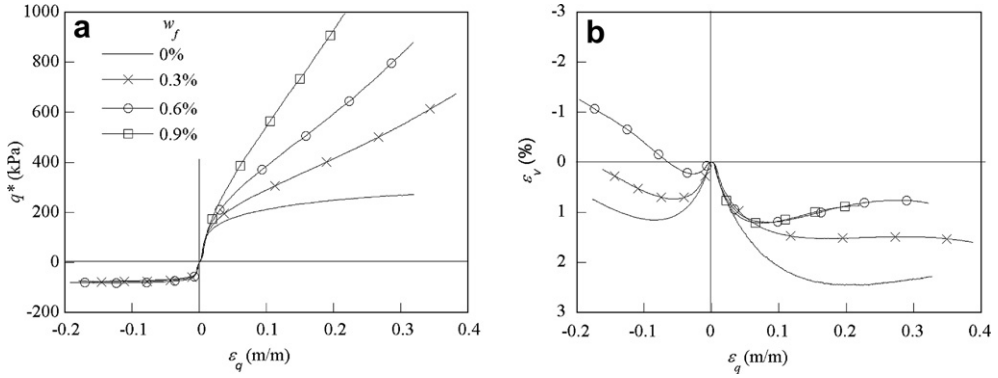

Fig. 5. Deviator stress–shear strain and volumetric behaviour for drained compression and extension triaxial tests on isotropically consolidated specimens at 100 kPa consolidation pressure (w_f represents the fibre content).

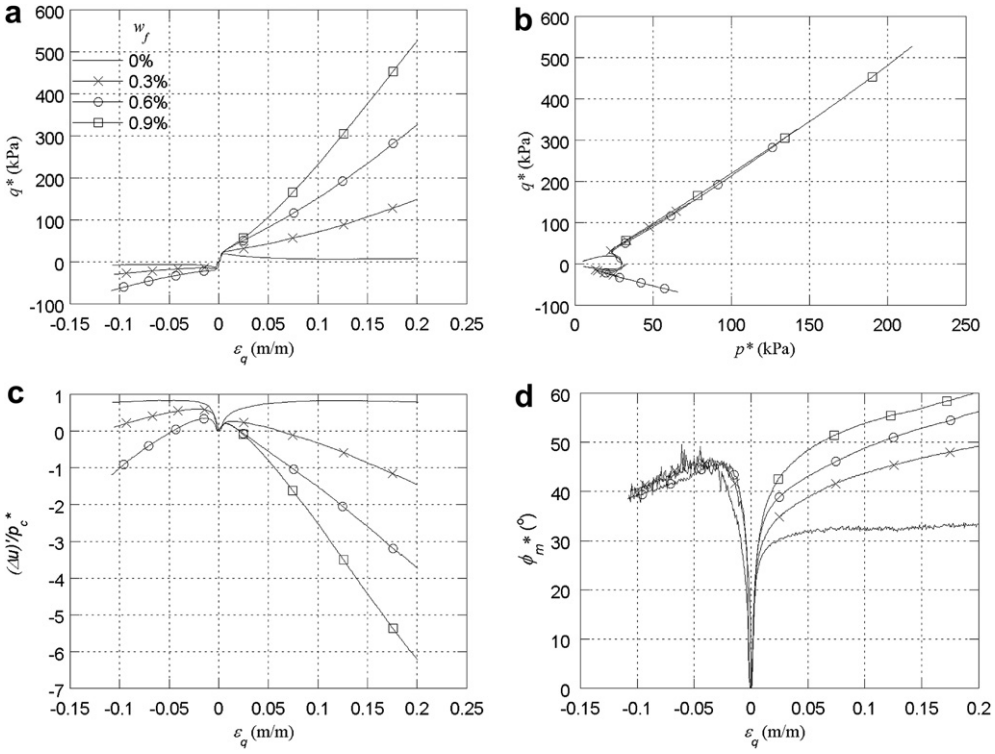

Fig. 6. Triaxial undrained compression and extension tests; 30 kPa initial consolidation pressure.

4.3. Undrained triaxial tests

Undrained monotonic compression and extension triaxial tests have been performed under the conditions listed in Table 2. The test results for reinforced and unreinforced specimens, and their dependence on the consolidation pressures, are shown in Figs. 6–8 for consolidation pressures of 30, 100 and 200 kPa respectively. Each of these figures shows: (a) the stress – strain response in terms of q^*:ε_q (note that $\varepsilon_q = \varepsilon_a$ for undrained deformation); (b) the effective stress path for the composite in the (q^*:p^*) plane; and the evolution with the shear strain of: (c) the effective stress part of the excess pore pressure $(\Delta u)'$, with $(\Delta u)' = \Delta u - \Delta p$ normalised by the effective mean consolidation stress, p_c^*, and (d) the composite effective mobilised angle of friction, ϕ_m^*. The use of $(\Delta u)'$ is instructive because it shows only the pore pressure resulting from the suppressed volume change of the soil, and subtracts the pore pressure change resulting from the imposed changes in total stress (which has nothing to do with the response of the soil).

4.3.1. Unreinforced specimens

In compression, as well as in extension, the specimens show a progressive generation of pore pressure and continuous decrease of effective mean stress acting on the sand. After a peak is reached rapidly near the start of the test there is a sharp drop of deviator stress and stabilisation around a steady state as deformation continues: behaviour typical of static liquefaction. The occurrence of liquefaction is observed even for specimens consolidated at the very low stress level of 30 kPa. The effective stress part of the excess pore pressure $(\Delta u)'$ developed progressively and reached a constant value at a shear strain of about 10% in compression and −5% in extension. The highest pore pressure increase in extension as well as in compression is about 85% of p_c^*.

The mobilised angle of friction at the peak deviator stress for the extension tests shows some dependency on the effective confining pressure with 19.8°, 19.6° and 18.2° for 30, 100 and 200 kPa respectively and this pattern is equally shown by the compression tests with 22.6°, 21.9° and 20.2° for the same successive effective consolidation pressures. However, both series of angles appear much higher than those obtained by Doanh et al. (1997) where an average of 12.7° for extension and 16.8° for compression for effective confining pressures ranging from 50 to 300 kPa were obtained: possibly, the present study has used slightly higher specimen densities.

The slope $M_c^{ss} = q^*/p^*$ of the steady state line in compression is about 1.38 and the corresponding maximum mobilised angle of friction is around 34° (close to that found by Doanh et al., 1997). In extension, the stress ratio $M_e^{ss} = q^*/p^*$ at the steady state of deformation is around −0.97 and the corresponding mobilised angle of friction tends towards 35° which is slightly higher than in compression.

4.3.2. Fibre reinforced specimens

When different concentrations of fibres are used as inclusions, the undrained behaviour of the reinforced specimens appears qualitatively very coherent from one group of tests to another. The presence of fibres – irrespective of the amount employed and the initial consolidation pressure – strongly affects the undrained response. Static liquefaction is fully prevented in compression with a behaviour comparable to that of a dense unreinforced sand. In extension there is a clear increase of both undrained peak and steady state shear strength response for low fibre concentrations and a strain hardening response for higher values of w_f (Figs. 6–8).

Any initial effects of imperfect contacts between the loading ram and specimen top platen are quickly erased as loading continues. The responses observed for both compression and extension loadings are very similar and follow quite closely the responses of the unreinforced specimens over the small strain domain in all planes (Figs. 6–8). This suggests that the initial

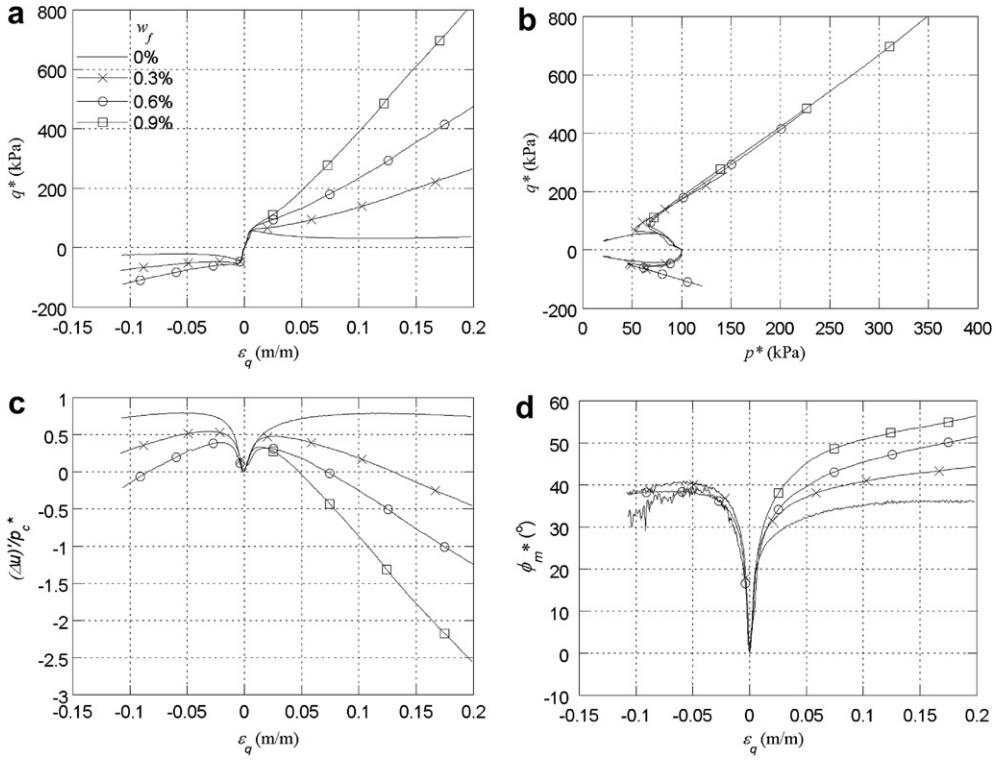

Fig. 7. Triaxial undrained compression and extension tests; 100 kPa initial consolidation pressure.

behaviour of the composite is to a certain extent solely controlled by the sand matrix (Heineck et al., 2005; Yetimoglu et al., 2005; Ibraim and Maeda, 2007). For a given consolidation pressure, further shearing in compression induces a monotonic increase of the undrained deviator stress that is highly dependent on the amount of the fibres employed, while in extension, for a fibre content $w_f = 0.3\%$, the deviator stress still exhibits a softening behaviour after reaching a peak (although the peak is slightly

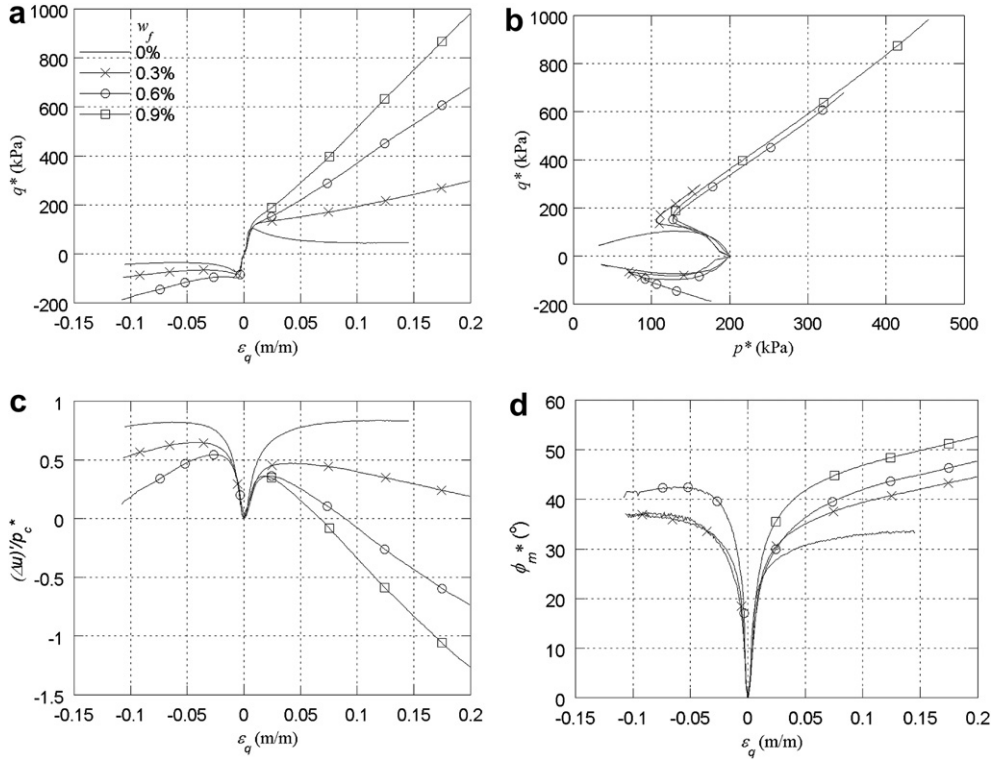

Fig. 8. Triaxial undrained compression and extension tests; 200 kPa initial confining pressure.

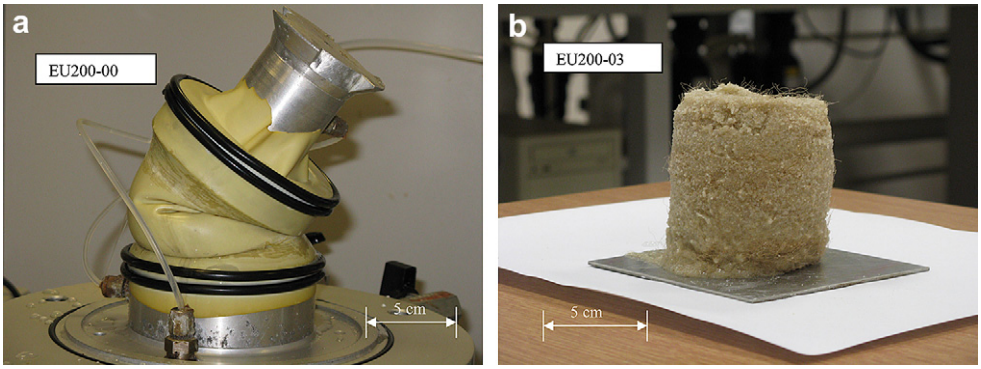

Fig. 9. Two photos of fully liquefied specimens due to a reversal axial straining at the end of the unloading extension tests: (a) unreinforced specimen; (b) reinforced specimen 0.3% fibre content.

higher than that of an unreinforced specimen), followed then by hardening (Figs. 6a, 7a, 8a). The undrained deviator peak observed in extension for the unreinforced and reinforced specimens ($w_f = 0.3\%$) vanishes for a fibre content of 0.6% and the deviator stress increases monotonically similar to the compressive response.

In compression as well as in extension, the undrained stress paths of the composite specimens in the (q^*:p^*) plane initially follow closely the stress path of the unreinforced one but at certain points the stress paths change direction sharply and show rapid increases in p^* axis and follow somewhat straight trajectories (Figs. 6b, 7b, 8b). For the same confining pressure, these trajectories appear to have the same slope independent of fibre concentration. However, straight lines that best fit each trajectory do not intersect the origin of axes either in compression or extension: a negative q^* axis offset intercept (much higher in absolute value in compression) is found systematically for all the consolidation pressures.

The pore pressure response of the reinforced specimens in compression as well as in extension typically show an initial increase in $(\Delta u)'/p_c^*$ ratio up to a peak level (significantly affected by the presence of fibres) followed by a decrease which, for some amounts of fibres, can even become negative (Figs. 6c, 7c, 8c), indicating a switch from suppressed contraction to suppressed dilation. For a given consolidation pressure, the rate at which $(\Delta u)'$ decreases with continued straining is lower in extension than in compression and higher for higher fibre concentrations. For a given fibre content, the rate at which $(\Delta u)'/p_c^*$ decreases following the peak is lower for higher consolidation pressures.

The mobilised angle of friction, ϕ_m^*, of the specimens reinforced with 0.3–0.9% of fibres in compression increases monotonically with the shearing and, at 20% of shear strain, respectively ranges from 49° to 60° for 30 kPa consolidation pressure, from 44° to 56° for 100 kPa and from 44° to 52° for 200 kPa (Figs. 6d–8d and Table 2). It can be observed that for a given fibre concentration, the mobilised angle of friction is higher for lower values of the consolidation pressure. In extension, for all fibre contents and consolidation pressures, the range of the mobilised angle of frictions at 10% of shear strain presents a narrow variation with values around $40 \pm 3°$.

Given the strict definition of liquefaction, a complete monotonic loading liquefaction was not attained as can be observed for any of the unreinforced specimens tested in this study, either in compression or in extension. Full liquefaction is possible, however, for unreinforced and reinforced specimens by applying a strain reversal (implying a sudden 90° rotation of principal strain axes) at the end of the monotonic loading. Fig. 9 shows pictures of the fully liquefied specimens: the unreinforced specimen (Fig. 9a) clearly shows a completely collapsed structure, while the reinforced one (Fig. 9b) is still able to maintain some structural stability even after the removal of the membrane. Considering that one of the consequences of liquefaction is the lateral spreading of the soil, it seems that the presence of fibres can limit or even prevent the occurrence of this phenomenon.

4.3.3. Characteristic states

The undrained effective stress paths for medium dense and dense sands typically include a point of vertical tangency, $\delta p'/\delta q' = 0$, which corresponds to the switch from suppressed contraction to suppressed dilation. This is similar to the so-called characteristic state (Luong, 1980) which also refers to a stress state corresponding to the transition from a contractive response to a dilative one. However, Luong originally defined the characteristic state (stress state corresponding to a volumetric strain increment $d\varepsilon_v = 0$) based on conventional drained compression triaxial tests which certainly implies that there might be some stress path dependency. There may be some similarity between the characteristic stress state that we are deducing from the shape of the undrained effective stress path and the so-called 'phase transformation' stress ratio introduced by Ishihara et al. (1975). This particular state can be identified in a (q':p') undrained effective stress path as the point where the effective mean stress reaches a minimum value and the tangent is parallel to the q' axis. The

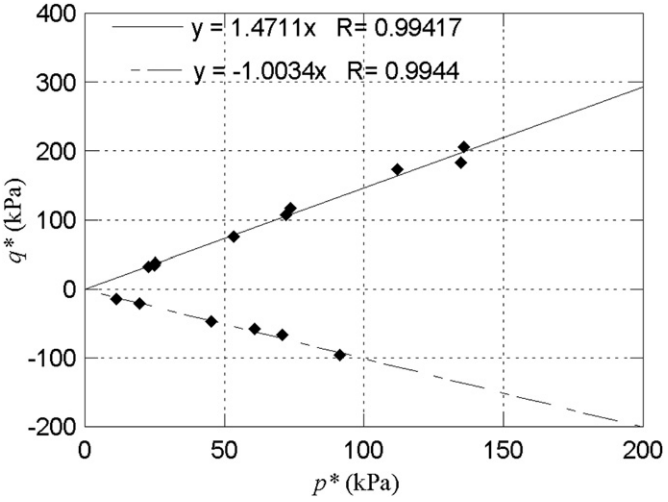

Fig. 10. Position of the point of phase transformation/characteristic states in the (q^*:p^*) stress plane for all the triaxial tests in compression and extension on reinforced specimens.

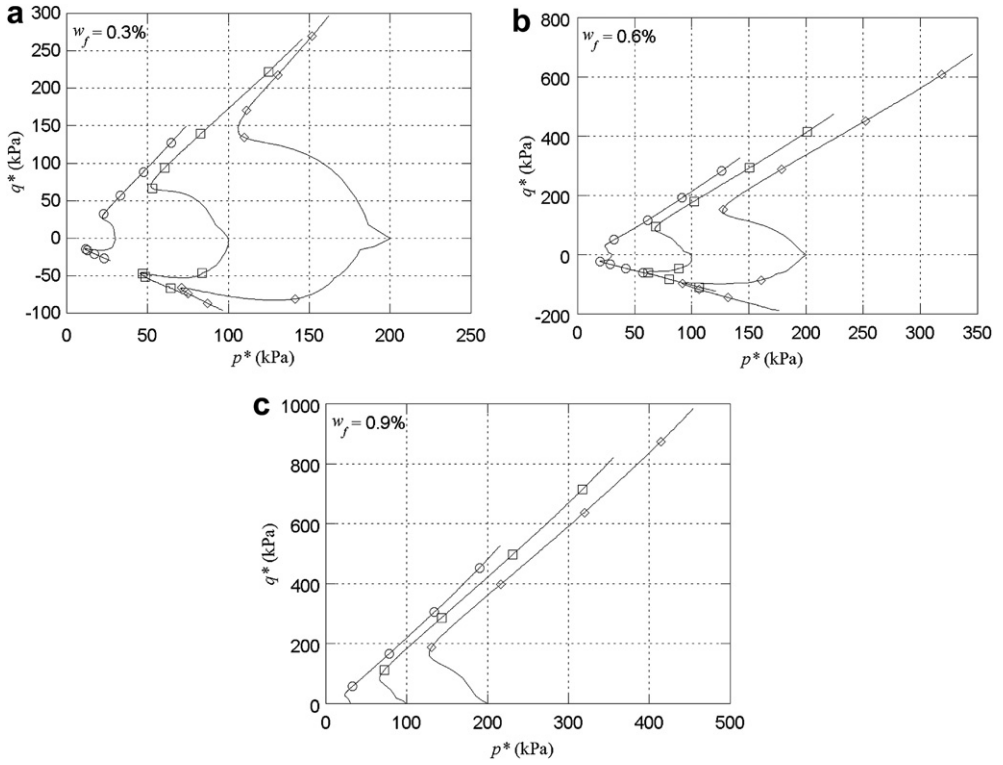

Fig. 11. Triaxial undrained compression and extension stress paths of tests on isotropically consolidated specimens to different consolidation pressures, p_c^*: (a) $w_f = 0.3\%$; (b) $w_f = 0.6\%$; (c) $w_f = 0.9\%$.

definition of the characteristic state in this way is therefore independent of the total stress path.

The positions of these characteristic state points for all the reinforced specimens in compression and in extension in the (q^*:p^*) stress plane are shown in Fig. 10. Irrespective of the fibre contents and initial consolidation pressures used in this study, the characteristic states can be well fitted in compression as well as in extension by two straight lines (with good regression coefficients)

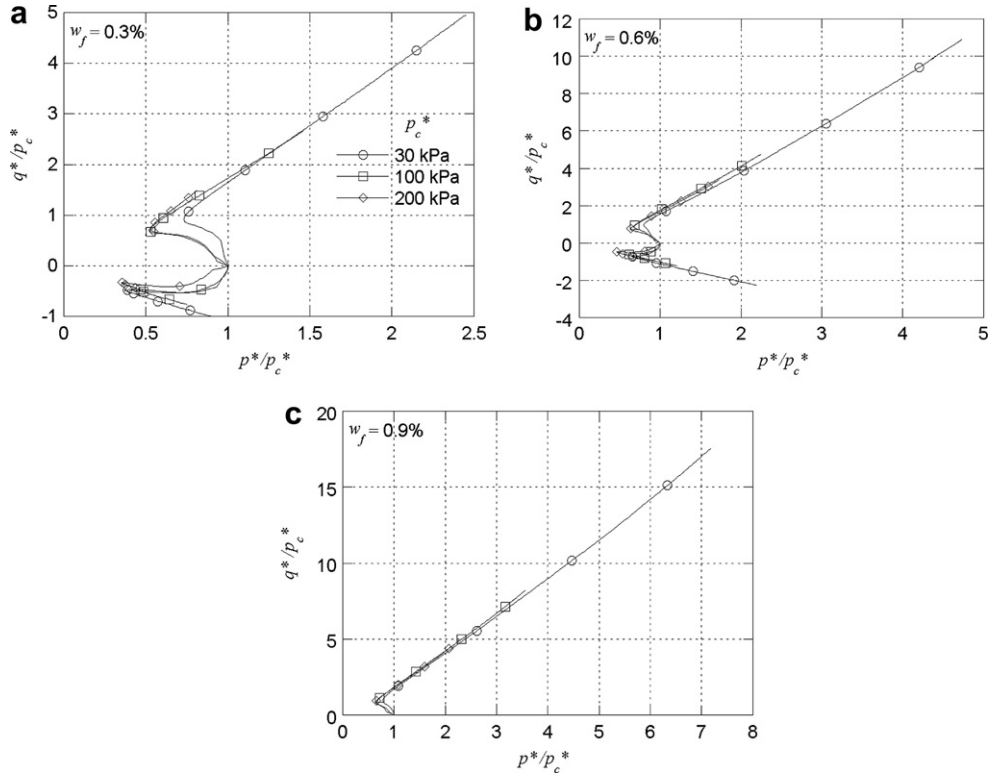

Fig. 12. Effective stress paths (q^*:p^*) normalised with the effective mean consolidation pressure, p_c^*: (a) $w_f = 0.3\%$; (b) $w_f = 0.6\%$; (c) $w_f = 0.9\%$.

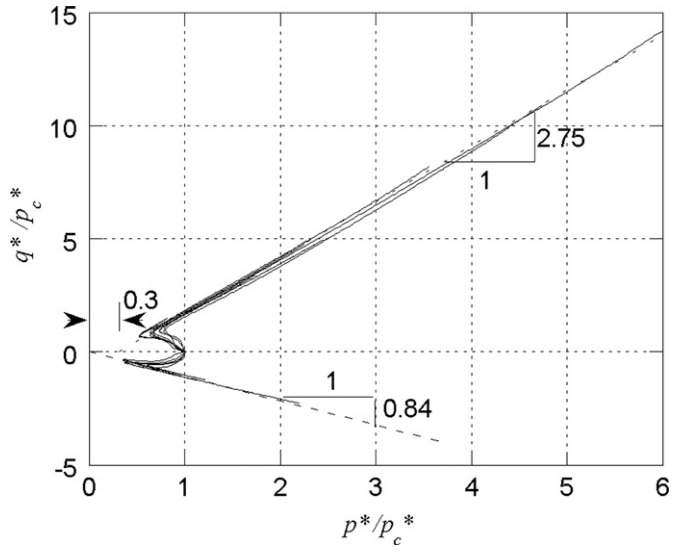

Fig. 13. Effective stress path (q^*:p^*) normalised with the effective mean consolidation pressure, p_c^*, of all tests on reinforced specimens.

passing through the origin of the (q^*:p^*) axes with slopes of 1.47 in compression and −1.00 in extension. The corresponding mobilised angles of friction are 36.2° in compression and 36.9° in extension.

4.3.4. Normalised stress paths

The stress paths in the (q^*:p^*) plane for tests on specimens reinforced with identical amounts of fibres but consolidated to different values of effective mean stress p_c^*, are shown in Fig. 11. On the compression side, and for one fibre content, the linear effective stress paths developed after the characteristic state run practically parallel to each other, with a higher intercept on the positive p^* axis (or lower intercept on the negative q^* axis) for higher consolidation pressures. In extension, Fig. 11a and b, a close examination of the stress paths may show a similar pattern but the distances between these parallel lines and the negative q^* axis intercept are both extremely small: therefore a common line passing through the origin of (q^*:p^*) axes could well approximate these linear stress paths. When these effective stress paths are normalised with p_c^* (Fig. 12) it appears that all the linear paths fall onto an identical straight line, unaffected by the proportion of fibres: Fig. 13 groups all the normalised stress paths of all the undrained tests performed in this study. In compression, its slope is approximately 2.75 and its intercept with the p^*/p_c^* axis occurs at a value of around 0.3 while in extension the slope is around −0.84.

4.3.5. Fibre stress contribution

The incremental stress–strain relationship for a reinforced soil, with the volume of fibres very small compared to the volume of the composite, is summarised in the Appendix (Diambra et al., in press, 2008b; Diambra, in press). Such a relationship can be used to separate the contributions of the sand and the fibres to the behaviour of the composite. The data in Figs. 6–8 and 11 have been accordingly re-analysed to show that, once the contribution of fibres has been taken out of the composite (q^*:p^*) stresses (curves marked with hollow symbols in Fig. 14), leaving only the (q':p') stresses acting on the sand component (curves with solid symbols in Fig. 14), the data at large shear strains collapse onto a unique line irrespective of fibre content and initial stress conditions. The slope is about 1.30 in triaxial compression and −0.93 in triaxial extension, corresponding very closely to a large strain friction angle of 33°, of the order normally expected for unreinforced Hostun RF sand. A critical (steady) state condition in the sand composite is nicely recovered.

5. Summary and conclusions

The analysis of the triaxial compression and extension tests on fibre reinforced and unreinforced sand specimens has revealed a number of points of interest.

- In trying to understand the behaviour observed in all triaxial tests it is important to take into account the actual somewhat sub-horizontal fibre orientations generated by the fabrication process. The drained test results clearly show that the strength increase contributed by the presence of fibres is highly anisotropic. This actual fibre orientation is specifically included in the model summarised in the Appendix. Qualitative awareness of this actual orientation is needed to appreciate the difference in response in compression and extension.
- Although the stress–strain response in extension is not much influenced by the presence of the sub-horizontal fibres (strength response rather dominated by the sand matrix), the volumetric behaviour in both compression and extension loading is significantly affected – even though the void ratio does not change significantly when fibres are added (see Table 2). These results clearly suggest that the volumetric response of the composite could be a consequence of an apparent densification of the sand matrix resulting from the presence of the fibres in the voids: the fibres appear to steal some of the voids from the sand. This idea is supported by the results of a constitutive model proposed by Diambra et al. (2008b).
- The presence of fibres clearly affects the undrained behaviour in compression as well as in extension and converts a strain

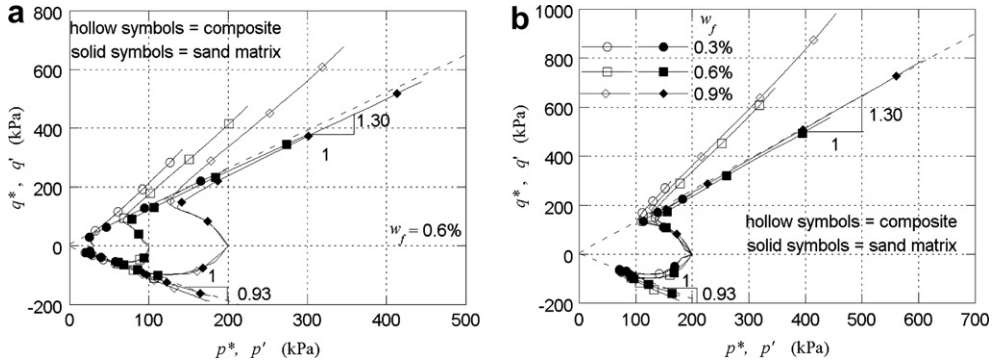

Fig. 14. Effective stress paths (q^*:p^*) of composite and (q':p') of sand matrix in triaxial compression and extension for (a) 0.6% fibre content and different consolidation pressures (30, 100 and 200 kPa) and (b) for 200 kPa consolidation pressure and different fibre contents, w_f (0.3, 0.6 and 0.9%). Hollow symbols represent data before adjustment (i.e. composite stresses). Solid symbols represent data after adjustment (i.e. stresses in the sand component of the composite).

softening response (typical for a loose unreinforced sand) into a strain hardening response. Static, or monotonic loading liquefaction appears to be prevented for both loading conditions but a higher concentration of fibres is needed for the prevention of liquefaction in extension. Normalisation of the stress paths with the mean effective stress at the end of consolidation shows a common path once the characteristic state is reached irrespective of the fibre concentration. The mobilised angles of friction coming from the slopes of the stress paths at large strains are vastly different for compression and extension and this is a consequence of the anisotropic nature of the distribution of fibre orientations. The angle of friction of reinforced specimens mobilised at the characteristic state appears independent of the fibre contents and initial consolidation pressure conditions used in this study, as well as the loading conditions (compression/extension).

- While full sample liquefaction is possible for unreinforced and reinforced specimens by applying a strain reversal (implying a sudden 90° rotation of principal strain axes) at the end of the monotonic loading, it seems that the presence of fibres can limit or even prevent the occurrence of the lateral spreading of the soil as normally observed for unreinforced samples.
- Analytical developments based on the tensile stress contribution of fibres and including the key aspect of fibre orientation distribution have shown that it is possible to convert the stresses acting on the composite, which are the stresses measured directly in the experiments, to the stresses acting on the sand component of the composite. Once the contribution of fibres has been taken out of the composite stresses, the experimental data for all the tests at large shear strains nicely collapse onto a unique line corresponding very closely to the mobilised steady state or critical state angle of friction of the tested sand. The stresses acting on the sand matrix may be scrutinised in the usual way when looking for behavioural characteristics such as formations of critical states or limiting compression lines.
- Practical application of the use of flexible fibres to improve the liquefaction resistance of real soils will evidently require consideration of large scale methods of preparation of the sand–fibre mixtures and the possible costs of any compaction procedures used to produce particular initial densities. These issues lie beyond the scope of the research presented in this paper which is part of an overall campaign to develop reliable constitutive models to describe the mechanical behaviour of the mixtures.

Acknowledgements

Financial support for this work was provided by the University of Bristol. This work benefitted from contacts that Erdin Ibraim and Andrea Diambra made with experts in the field; this was possible with financial support from Royal Academy of Engineering (UK) through the International Travel Grant Scheme. The Loksand™ fibres were kindly provided by Drake Extrusion Ltd (UK).

Appendix. Fibre stress contribution

The incremental stress–strain relationship for a reinforced soil may be written as (Diambra et al., in press, 2008b; Diambra, in press):

$$\dot{\boldsymbol{\sigma}}^{*} = v_{\mathrm{m}}\dot{\boldsymbol{\sigma}}' + v_{\mathrm{f}}\dot{\boldsymbol{\sigma}}_{\mathrm{f}} = [M_{\mathrm{m}}]\dot{\boldsymbol{\varepsilon}} + v_{\mathrm{f}}\left[M_{\mathrm{f}}\right]\dot{\boldsymbol{\varepsilon}} \tag{A1}$$

where $[M_{\mathrm{m}}]$ is the stiffness matrix for the sand, $[M_{\mathrm{f}}]$ is the stiffness matrix for the fibres, and v_{m} and v_{f} are respectively the volumetric concentrations of the sand matrix and fibres as defined by (4). v_{f} is directly related to w_{f} (fibre concentration by dry weight of sand) through the following relationship: $v_{\mathrm{f}} = (G_{\mathrm{s}}/G_{\mathrm{f}})w_{\mathrm{f}}/(1+e_{\mathrm{m}})$, where e_{m} is the void ratio when the volume of fibres is 'attached' to the volume of voids.

When conventional triaxial $p-q$ notations are adopted, and when fibre orientation distribution is symmetrical with respect to the vertical axis, $v_{\mathrm{f}}\dot{\boldsymbol{\sigma}}_{\mathrm{f}}$ may be written in the expanded form (Diambra et al., in press):

$$v_{\mathrm{f}}\begin{bmatrix}\dot{p}_{\mathrm{f}}\\ \dot{q}_{\mathrm{f}}\end{bmatrix} = E_{\mathrm{f}}f_{\mathrm{b}}\begin{bmatrix}M_{11} & M_{12}\\ M_{21} & M_{22}\end{bmatrix}\begin{bmatrix}\dot{\varepsilon}_{\mathrm{p}}\\ \dot{\varepsilon}_{\mathrm{q}}\end{bmatrix} \tag{A2}$$

where E_{f} is the Young's modulus of the fibres, f_{b} is a dimensionless fibre sliding function ($f_{\mathrm{b}}=1$ for perfect bonding between fibres and sand and $f_{\mathrm{b}}=0$ for full sliding),
$M_{11} = (1/9)(F_{11}+F_{12}+2F_{21}+2F_{22})$,
$M_{12} = (1/3)(F_{11}-(F_{12}/2)+2F_{21}-F_{22})$,
$M_{21} = (1/3)(F_{11}+F_{12}-F_{21}-F_{22})$,
$M_{22} = (1/2)(2F_{11}-F_{12}-2F_{21}+F_{22})$ and the F_{ij} terms represent the components of the matrix:

$$\begin{bmatrix}\int_{\alpha_1}^{\alpha_2}\rho(\theta)\cos(\theta)\sin^4(\theta)\mathrm{d}\theta & \int_{\alpha_1}^{\alpha_2}\rho(\theta)\cos^3(\theta)\sin^2(\theta)\mathrm{d}\theta\\ \frac{1}{2}\int_{\alpha_1}^{\alpha_2}\rho(\theta)\cos^3(\theta)\sin^2(\theta)\mathrm{d}\theta & \frac{1}{2}\int_{\alpha_1}^{\alpha_2}\rho(\theta)\cos^5(\theta)\mathrm{d}\theta\end{bmatrix} \tag{A3}$$

in which $\rho(\theta)$ is the fibre orientation distribution function that can be defined based on the experimental and analytical developments of Diambra et al. (2007b). The integration limits in (A3) are $\alpha_1=0$ and $\alpha_2=\theta_0$ for compression loading and $\alpha_1=\theta_0$ and $\alpha_2=\pi/2$ for extension loading, where $\theta_0=\arctan\sqrt{-\dot{\varepsilon}_{\mathrm{r}}/\dot{\varepsilon}_{\mathrm{a}}}$ is the direction of zero incremental strains.

Following Diambra et al. (2008b, in press) and Diambra (in press), it is assumed that

$$f_{\mathrm{b}} = 0.6\left(1-\exp\left(-0.75\frac{p^{*}}{p_{\mathrm{ref}}}\right)\right) \tag{A4}$$

$$\rho(\theta) = v_{\mathrm{f}}\frac{0.43|\cos(\theta)|}{1.04-0.83\cos(\theta)^2} \tag{A5}$$

with $p_{\mathrm{ref}}=100$ kPa a reference pressure. The dependency of f_{b} on p^{*} allows the replication of an enhanced bonding between fibres and sand matrix at higher confining stresses as observed in the experiments (Diambra et al., in press).

Using these relations it is possible to convert the stresses acting on the composite (p^{*} and q^{*}), which are the effective stresses measured directly in the experiments (after taking pore pressures into account), to the stresses acting on the sand component of the composite (p' and q') in the following incremental form:

$$\begin{aligned}\dot{p}' &= \dot{p}^{*} - E_{\mathrm{f}}f_{\mathrm{b}}(M_{11}\dot{\varepsilon}_{\mathrm{p}}+M_{12}\dot{\varepsilon}_{\mathrm{q}}) \text{ and}\\ q' &= \dot{q}^{*} - E_{\mathrm{f}}f_{\mathrm{b}}(M_{21}\dot{\varepsilon}_{\mathrm{p}}+M_{22}\dot{\varepsilon}_{\mathrm{q}})\end{aligned} \tag{A6}$$

The results in Figs. 5–7 and 9 have been re-analysed and the contribution of fibres extracted according to (A6), with $E_{\mathrm{f}}=900$ MPa, shown in Fig. 12.

References

Al Refeai, T.O., 1991. Behaviour of granular soils reinforced with discrete randomly oriented inclusions. Geotextiles and Geomembranes 10, 319–333.
Arthur, J.R.F., Chua, K.S., Dunstan, T., 1980. Principal stress rotation a missing parameter. Journal of the Geotechnical Engineering Division, ASCE 106 (4), 419–433.

Bjerrum, L., Kringstad, S., Kummeneje, D., 1961. The shear strength of a fine sand. In: Proceedings of 5th International Conference on Soil Mechanics and Foundation Engineering, Paris, vol. 1, pp. 29–37.
Boominathan, A., Hari, S., 2002. Liquefaction strength of fly ash reinforced with randomly distributed fibres. Soil Dynamics and Earthquake Engineering 22, 1027–1033.
Castro, G., 1969. Liquefaction of Sand. Ph.D. thesis, Harvard Soil Mechanics Series N° 81, Harvard University, Cambridge, MA, 112 pp.
Castro, G., Christian, J.T., 1976. Shear strength of soils and cyclic loading. Journal of Geotechnical Engineering Division, ASCE 102 (GT9), 887–894.
Castro, G., Poulos, S.J., 1977. Factors affecting liquefaction and cyclic mobility. Journal of Geotechnical Engineering Division, ASCE 103 (GT6), 501–516.
Chu, J., 1991. Liquefaction of sands under undrained and non-undrained conditions. In: Proceedings of 5th International Conference on Soil Dynamics and Earthquake Engineering, Karlsruhe, Germany, pp. 277–291.
Consoli, N.C., Prietto, P.D.M., Ulbrich, L.A., 1998. Influence of fiber and cement addition on behaviour of sandy soil. Journal of Geotechnical and Geoenvironmental Engineering, ASCE 124 (12), 1211–1214.
Consoli, N.C., Heineck, K.S., Casagrande, M.D.T., Coop, M.R., 2007. Shear strength behavior of fiber-reinforced sand considering triaxial tests under distinct stress paths. Journal of Geotechnical and Geoenvironmental Engineering, ASCE 133 (11), 1466–1469.
Consoli, N.C., Festugato, L., Heineck, K.S., 2009. Strain-hardening behaviour of fibre-reinforced sand in view of filament geometry. Geosynthetics International 16 (2), 109–115.
Danjon, F., Barker, D.H., Drexhage, M., Stokes, A., 2007. Using three-dimensional plant root architecture in models of shallow–slope stability. Annals of Botany, 1–13.
Diambra, A. Fibre reinforced sands: experiments and constitutive modelling. PhD thesis, University of Bristol, in press, doi:10.1016/j.geotexmem.2009.09.010.
Diambra, A., Russell, A.R., Ibraim, E., Muir Wood, D., 2007a. Determination of fibre orientation distribution in reinforced sand. Géotechnique 57 (7), 623–628.
Diambra, A., Ibraim, E., Russell, A.R., Muir Wood, D., 2007b. Shear tests on fibre reinforced sands. In: Proceedings of 5th International Symposium on Earth Reinforcement, IS Kyushu2007, Japan, Balkema. Taylor & Francis Ed., pp. 329–334.
Diambra, A., Ibraim, E., Muir Wood, D., Russell, A.R., Bennani, Y., 2008a. Effect of sample preparation on the behaviour of fibre reinforced sands. In: Proceedings of the 4th Int. Symposium on Deformation Characteristic of Geomaterials, IS-Atlanta 2008, USA, vol. 2. IOS Press, pp. 629–636.
Diambra, A., Ibraim, E., MUir Wood, D., Russell, A.R. Fibre reinforced sands: Experiments and modelling, Geotextiles and Geomembranes, in press, doi:10.1016/j.geotexmem.2009.09.010.
Diambra, A., Ibraim, E., Muir Wood, D., Russell, A.R., 2008b. Behaviour of reinforced sands: experiments and modeling. In: 19th European Young Geotechnical Engineers Conference, Hungary, pp. 1–10.
Doanh, T., Ibraim, E., Matiotti, R., 1997. Undrained instability of very loose Hostun sand in triaxial compression and extension. Part 1: experimental observations. Journal of Cohesive-Frictional Materials 2, 47–70.
Doanh, T., Ibraim, E., 2000. Minimum undrained strength of very loose Hostun RF sand in triaxial compression and extension. Géotechnique 50 (4), 377–392.
Ekanayake, J.C., Phillips, C.J., 2002. Slope stability thresholds for vegetated hillslopes: a composite model. Canadian Geotechnical Journal 39 (4), 849–862.
Gray, D.H., Al-Refeai, T.O., 1986. Behaviour of fabric – versus fiber-reinforced sand. Journal of Geotechnical Engineering 112 (8), 804–820.
Gray, D.H., Ohashi, H., 1983. Mechanics of fiber reinforcement in sands. Journal of Geotechnical Engineering Division, ASCE 109 (3), 335–353.
Greenwood, J.R., 2006. SLIP4EX – A program for routine slope stability analysis to include the effects of vegetation, reinforcement and hydrological changes. Geotechnical and Geological Engineering 24, 449–465.
Greenwood, J.R., Norris, J.E., Wint, J., 2004. Assessing the contribution of vegetation to slope stability. In: Geotechnical Engineering, Proceedings of the ICE, GE4, pp. 199–207.
Heineck, C.S., Consoli, N.C., Coop, M.R., 2005. Effect of microreinforcement of soils from very small to large shear strains. Journal of Geotechnical and Geoenvironmental Engineering, ASCE 131 (8), 1024–1033.
Hyodo, M., Tanimizu, H., Yasufuku, N., Murata, H., 1994. Undrained cyclic and monotonic triaxial behaviour of saturated loose sand. Soils and Foundations 34 (1), 19–32.
Ibraim, E., 1998. Différents aspects du comportement des sables à partir d'essais triaxiaux: des petites déformations à la liquéfaction statique. PhD thesis, ENTPE Lyon.
Ibraim, E., Muir Wood, D., Maeda, K., Hirabayashi, H., 2006. Fibre-reinforced granular soils: numerical approach. In: Hyodo, Murata, Nakata (Eds.), Proceedings of the International Symposium on Geomechanics and Geotechnics of Particulate Media, Ube, Yamaguchi, Japan. Taylor & Francis, London, pp. 443–448.
Ibraim, E., Fourmont, S., 2007. Behaviour of sand reinforced with fibres. In: Ling, Callisto, Leshchinsky, Koseki (Eds.), Soil stress–strain behaviour: measurement, Modelling and Analysis, Geotechnical Symposium, Rome, March 16–17. Springer, pp. 807–918.
Ibraim, E., Maeda, K., 2007. Numerical analysis of fibre-reinforced granular soils. In: Proceedings of 5th International Symposium on Earth Reinforcement, IS Kyushu2007, Japan, Balkema. Taylor & Francis Ed., Balkema, pp. 387–393.
Ishihara, K., Tatsuoka, F., Yasuda, Y., 1975. Undrained deformation and liquefaction of sand under cyclic stresses. Soils and Foundations 15 (1), 29–44.
Jewell, R.A., Wroth, C.P., 1987. Direct shear tests on reinforced sand. Géotechnique 37 (1), 53–68.
Konrad, J.M., 1990. Minimum undrained strength of two sands. Journal of Geotechnical Engineering, ASCE 116 (6), 932–947.
Kramer, L., Seed, H.B., 1988. Initiation of soil liquefaction under static loading conditions. Journal of Geotechnical Engineering 114 (4), 412–430.
Krishnaswamy, N.R., Isaac, N.T., 1994. Liquefaction potential of reinforced sand. Geotextiles and Geomembranes 13 (1), 23–41.
Lade, P.V., 1992. Static instability and liquefaction of loose fine sandy slopes. Journal of Geotechnical Engineering 118 (1), 51–71.
Lade, P.V., 1993. Initiation of static instability in the submarine Nerlerk berm. Canadian Geotechnical Journal 30, 895–904.
Li, J., Ding, D.W., 2002. Nonlinear elastic behaviour of fiber-reinforced soil under cyclic loading. Soil Dynamics and Earthquake Engineering 22, 977–983.
Lindenberg, J., Koning, H.L., 1981. Critical density of sand. Géotechnique 31 (2), 231–245.
Luong, M.P., 1980. Stress–strain aspects of cohesionless soils under cyclic and transient loading. Microstructural Science 1, 315–324.
Maher, M.H., Gray, D.H., 1990. Static response of sand reinforced with fibres. Journal of Geotechnical Engineering, ASCE 116 (11), 1661–1677.
Maher, M.H., Ho, Y.C., 1994. Mechanical properties of kaolinite/fiber soil composite. Journal of Geotechnical Engineering Division, ASCE 120 (8), 1381–1393.
Maher, M.H., Woods, R.D., 1990. Dynamic response of sands reinforced with randomly distributed fibers. Journal of Geotechnical Engineering, ASCE 116 (7), 1116–1131.
Michałowski, R.L., 2008. Limit analysis with anisotropic fibre-reinforced soil. Géotechnique 58 (6), 489–501.
Michałowski, R.L., Zhao, A., 1996. Failure of fiber-reinforced granular soils. Journal of Geotechnical Engineering, ASCE 122 (3), 226–234.
Michałowski, R.L., Čermák, J., 2002. Strength anisotropy of fiber-reinforced sand. Computers and Geotechnics 29, 279–299.
Mohkam, M., 1983. Contribution à l'étude expérimentale et théorique du comportement des sables sous chargements cycliques. PhD thesis, l'USM and INP Grenoble.
Murray, J.J., Frost, J.D., Wang, Y., 2000. Behaviour of sandy silt reinforced with discontinuous recycled fibre inclusions. Transportation Research Record 1714, 9–17.
Noorany, I., Uzdavines, M., 1989. Dynamic behavior of saturated sand reinforced with geosynthetic fabrics. In: Proc., Geosynthetics '89 Conf., vol. II, San Diego, California, pp. 385–396.
Özkul, Z.H., Baykal, G., 2007. Shear behaviour of compacted rubber fiber–clay composite in drained and undrained loading. Journal of Geotechnical and Geoenvironmental Engineering, ASCE 133 (7), 767–781.
Palmeira, E.M., Milligan, G.W.E., 1989. Large scale direct shear tests on reinforced soil. Soils and Foundations 29 (1), 18–30.
Park, T., Ann Tan, S., 2005. Enhanced performance of reinforced soil walls by the inclusion of short fiber. Geotextiles and Geomembranes 23, 348–361.
Poulos, S.J., 1981. The steady state of deformation. Journal of Geotechnical Engineering 107 (GT5), 553–562.
Ranjan, G., Vasan, R.M., Charan, H.D., 1996. Probabilistic analysis of randomly distributed fiber-reinforced soil. Journal of Geotechnical Engineering, ASCE 122 (6), 419–426.
Santoni, R.L., Webster, S.L., 2001. Airfields and roads construction using fibre stabilization of sands. Journal of Transportation Engineering 127 (2), 96–104.
Singh Chauhan, M., Mittal, S., Mohanty, B., 2008. Performance evaluation of silty sand subgrade reinforced with fly ash and fibre. Geotextiles and Geomembranes 26, 429–435.
Sivakumar Babu, G.L., Vasudevan, A.K., Haldar, S., 2008. Numerical simulation of fiber-reinforced sand behaviour. Geotextiles and Geomembranes 26, 181–188.
Sladen, J.A., D'Hollander, R.D., Krahn, J., Mitchell, D.E., 1985. Back analysis of Nerlerk berm liquefaction slides. Canadian Geotechnical Journal 22, 579–588.
Sway, A.T., Bang, S., 2007. Analysis of geofiber reinforced soils. In: Proceedings of 5th International Symposium on Earth Reinforcement, IS Kyushu2007, Japan, Balkema. Taylor & Francis Ed., pp. 357–362.
Tingle, J.S., Santoni, R.L., Webster, S.L., 2002. Full-scale field tests of discrete fibre-reinforced sand. Journal of Transportation Engineering 128 (1), 9–16.
Unnikrishnan, N., Rajagopal, K., Krishnaswamy, N.R., 2002. Behaviour of reinforced clay under monotonic and cyclic loading. Geotextiles and Geomembranes 20, 117–133.
Vaid, Y.P., Chern, J.C., 1983. Effect of static shear on resistance to liquefaction. Soils and Foundations 23 (1), 46–59.
Vercueil, D., Billet, P., Cordary, D., 1997. Study of the liquefaction resistance of a saturated sand reinforced with geosynthetics. Soil Dynamics and Earthquake Engineering 16, 417–425.
Wu, T.H., McOmber, R.M., Erb, R.T., Beal, P.E., 1988. Study of soil–root interaction. Journal of Geotechnical Engineering, ASCE 114 (12), 1351–1375.
Yetimoglu, T., Inanir, M., Esat Inanir, O., 2005. A study on bearing capacity of randomly distributed fiber-reinforced sand fills overlying soft clay. Geotextiles and Geomembranes 23, 174–183.
Yetimoglu, T., Salbas, M., 2003. A study on the shear strength of sands reinforced with randomly distributed discrete fibres. Geotextiles and Geomembranes 21, 103–110.
Zornberg, J.G., 2002. Discrete framework for equilibrium analysis of fibre-reinforced soil. Géotechnique 52 (8), 593–604.